Applied Physics B manuscript No.
(will be inserted by the editor)

Microscopic model for optical pattern and cavity soliton formation in a semiconductor Quantum Dot microresonator

I. M. Perrini[1], **S. Barbay**[2⋆], **T. Maggipinto**[1], **M. Brambilla**[1], **R. Kuszelewicz**[2]

[1] INFM, Dipartimento Interateneo di Fisica, Università e Politecnico di Bari, Via Orabona 4, 70126 Bari, Italy
[2] Laboratoire de Photonique et de Nanostructures, Route de Nozay, 91460 Marcoussis, France

The date of receipt and acceptance will be inserted by the editor

Abstract We develop a model that describes the optical response of a semiconductor quantum dot medium in a cavity in order to investigate pattern and cavity solitons formation. This model, beyond the inclusion of the inhomogeneous broadening of the quantum dot linewidth[1] (due the fluctuations of the quantum dot sizes that arise in self-organized growth), takes into account more complex phenomena such as the thermal escape and capture as well as Auger scattering mechanisms coupling the quantum dot itself with the wetting layer, and carrier diffusion in the unconfined directions of the wetting layer. We study the conditions for the onset of bistability and modulational instability and characterize the patterns formed at the bifurcated solutions. New features brought by these terms and indications on the most favourable regimes for cavity solitons formation are discussed.

1 Introduction

Since their first realisations in the early 1990's, quantum dots (QD) have raised a remarkable interest in the research fields concerned with material physics as well as nonlinear and quantum optics. Due to their 3D quantum confinement, QD are the sole to possess a discrete energy spectrum of bounds states. Therefore, from the viewpoint of optical transitions QD behave much like atoms. However, this comparison may not be pushed too far, essentially because in solids, quantum confinement is obtained as an over-modulation of a crystal potential. As a result, the confinement properties still coexist with the collective electronic properties. For example, one of the most common techniques for realising self-assembled QD is to use the Stransky-Krastanov growth regime where the QD sit on an ultra-thin 2D quantum well of a few atomic monolayers thickness called the wetting layer (WL). This introduces a coupling mechanism between the set of discrete energy levels of the QD and the WL continuum of states that sensibly modifies the light-matter interaction as compared to the atomic model. It is however true that QD provide an optical access to the high energy side of their electronic transitions at excitation regimes below transparency. This was not the case for bulk and quantum well systems, although pattern formation has been reported in such systems in the passive regime[2,3,4], and this considerably entailed the development of phenomena relying on the self-focusing effect. In the purely dispersive case, the sign of the nonlinear effect conditions the observation of temporal or spatial solitons[5,6]. A self-focusing nonlinearity was shown to be more favorable for the existence of the so-called Cavity Solitons (CS) [7]. CS are bistable localised optical states, independently writable and erasable in the transverse plane of a resonator with large Fresnel number filled with a nonlinear medium. They can be moved across the transverse plane by amplitude or phase gradients in the field profile. These properties makes them very promising candidates for massively parallel, all optical processing. Macroscopic systems with materials such as Liquid Crystal Light Valves [8,9] or Sodium vapor in a cell [10], have shown robust and controllable CS in large regions of their parameter space with modest energy requirements, owing essentially to the extremely favorable conditions brought by the strong positive Kerr effect exhibited by these materials.

The combination of such properties with the widely acknowledged potential of direct gap semiconductors for integration, miniaturisation and all-optical processing would constitute *per se* a breakthrough, making it possible a wealth of physical experiments and performing applications.

In a previous paper [1], we have developed a two-level model in order to determine the ability of QD to exhibit a strong saturable nonlinearity. Our primary concern was to evaluate the efficiency of the nonlinear optical response introduced by the presence of the inhomogeneous broadening resulting from fluctuations in the QD size. We have been able to determine the critical QD density ($N_c \simeq 10^{12} cm^{-3}$) for state-of-the-art InAs QD grown on a GaAs WL to achieve the onset of modulational instability (MI) that triggers pattern and CS formation in a microresonator. That model, though, included some strongly limiting approximations, as it only considered one electron-hole state and neglected all interactions between the dot itself and the WL on which it sits. The first assumption underestimated the strength of the non-

⋆ Corresponding author : sylvain.barbay@lpn.cnrs.fr

linear interaction, while accounting for spin-paired electrons should certainly result in a more favourable criterion for the MI threshold. The model refinements presented in this paper allow us to account for larger excitation intensities, which is compulsory if one wants to exploit optical nonlinearities. The introduction of the complex mechanisms of the QD-WL interactions is certainly less perspicuous on that issue, as it modifies the QD population and thus may decrease the nonlinear response and provide a spatial diffusion channel. It is the scope of the present paper to study the formation of pattern as well as the existence and robustness of Cavity Solitons, under the inclusion of such important aspects of QD materials. The theoretical/numerical indications will be essential in view of assessing the feasibility, and providing directions, for the experimental implementation of a QD CS forming microresonator, currently in progress at the LPN. We note that we consider QD having only one well-confined electron and hole state. This assumption is motivated by our primary goal to probe the two-level like susceptibility of QD and shall be discussed in section 2.

There have already been several approaches to the modelling of the optical response of semiconductor QD. Rate equations models [11,12] describe the mean population dynamics of a QD ensemble. Random population models use a master equation for microstates which describes the density of QD with a given population in interaction with a reservoir [13]. Averaging over the inhomogeneous linewidth, the authors can recover the absorption/gain of the medium and the phase response can be found by a Kramers-Kronig transformation. More sophisticated models [14,15,16,17,18] take into account the effects of the WL population that is believed to yield an important renormalization of the QD energy bandgap, but disregarding the microscopic dynamics of the carriers between the WL and the QD. This stationary and quasi-equilibrium approach neglects Auger processes coupling QD and WL carrier distributions, and leading to carrier diffusion through the WL with possible shortfalls on the MI and CS stability. Our approach, extends the one developed in [1] with an approach similar to that of Ref. [19], in the sense that we build a microscopic model of QD-Bloch equations including WL-QD interactions.

In doing so, we assume a spatially continuous and homogeneous QD medium and ignore band-gap renormalization effects as long as the WL population is low enough.Indeed, the analysis and the results performed throughout this work will concentrate on an unpumped configuration, where all carriers are generated by an external driving optical field, resonant with the QD fundamental transition. The model, however, lends itself to extension towards a regime of high WL carrier density (through an electric current or optical pumping in the WL), and this will be mentioned *en passant* in Sec.2.

This paper is organised as follows : we describe the theoretical model in section 2. Starting from the expressions of rate equations for carriers in a homogeneous population of QD, we extend it to the case of an inhomogeneously broadened population. The field equation is then introduced and the complete sets of equations written in terms of adimensional rescaled variables. We then perform a comparison between our electron-hole pair model [1] and the present one. In section 3, we characterize the system's optical properties, and study the pattern-formation domains and CS. Finally, the MI threshold conditions are obtained and analysed as a function of the various parameters determining the QD-WL interactions. The conclusion summarizes the results obtained and opens some perspectives concerning the use of semiconductor QD as a passive nonlinear medium for CS formation.

2 Model

2.1 Identical quantum dots

Semiconductor QD have discrete energy levels thanks to the spatial confinement of carriers. Energy levels are highly dependent on the QD geometry, the strain between the dot and the host material, and on the materials involved. It is then difficult to build a model without some general (and reasonable) assumptions on the electronic structure of the QD.

In this work we consider only the QD fundamental transition coupled to the WL. This situation constitutes the best system for the observation of two-level features in QD that is the concern of this work. Our model can apply e.g. to small and/or shallow confined QD so that either there is only one electron and one hole bound states, or the other discrete states, if any, are well separated from the inhomogeneously broadened fundamental transition and very close to the WL continuum states. The WL and eventually additional discrete sates are thus not expected to contribute significantly to the optical susceptibility in the vicinity of the fundamental transition. Intraband transitions between the QD and the WL, which were recently shown [20,21] to contribute significantly to the optical susceptibility in certain energy ranges, will also be neglected for the sake of simplicity and because the general impact of such contribution needs further theoretical and experimental investigations.

In QD, relaxation mechanisms are complex and not fully understood yet. Nevertheless, we shall incorporate them in our model through phenomenological escape and capture transition rates. Following our assumptions for the model, we shall consider only the WL-QD interactions. The spin dynamics is neglected since the spin memory is lost very fast at room temperature (some ps[22,23]). The coupling mechanisms between the WL and the QD are twofold. On the one hand carriers can escape or be captured by the dot via thermoactivation through emission or absorption of lattice phonons. Thermo-emission and capture mechanisms are important and fast relaxation mechanisms at room temperature. The typical timescales involved are in the range of 1 to 10ps. On the other hand, Auger processes, involving three particles, can also participate to the carrier exchanges between the QD and the WL [24]. They are believed to be particularly important for properly describing QD laser dynamics, especially if the WL population is large. We will only investigate passive or weakly pumped QD so that we may assume that the WL pop-

ulation is small as compared to the situation of current injection or optical pumping populating the dots through the WL. We therefore retain only those Auger processes implying first order contributions in the WL population. These Auger processes correspond to a situation where an electron and a hole are ejected from the QD and a carrier in the WL gains energy, or to the symmetric processes with respect to electrons and holes. Finally, elastic diffusion of WL and QD electrons and holes (not changing the occupation number, i.e. involving virtual transitions) contributes to the dipole dephasing, responsible for the large homogeneous linewidth of QD, and to a shift of the energy levels which can be included into the transition energies (see [25]).

We start from the single particle semiconductor equations (see e.g. [26]) where $n^{e,h}$ are the expectation values of the number of particles operator for the electrons and holes and p is the corresponding polarization :

$$\frac{dn^{e,h}}{dt} = -\gamma_{nr} n^{e,h} - \Gamma_{sp} n^e n^h + \frac{i}{\hbar}(dp^* - d^* p)\mathsf{E} + \left.\frac{dn^{e,h}}{dt}\right|_{QD-WL} + \left.\frac{dn^{e,h}}{dt}\right|_{QD-WL}^{Auger} \quad (1)$$

$$\frac{dp}{dt} = -\left(i\omega_a + \gamma_p\right) p - \frac{i}{\hbar}\left[n^e + n^h - 1\right] d\mathsf{E}. \quad (2)$$

The parameters are γ_{nr} the non radiative recombination rate, Γ_{sp} the bimolecular coefficient for spontaneous recombination, ω_a the electron-hole recombination pulsation, γ_p the polarization damping, $\mathsf{E} = E\exp(-i\omega_0 t) + c.c.$ is the electric field and d the dipole transition matrix element.

The quantum dot occupation number for the electrons and holes is given by the sum over opposite spins of the single particle states $n^{e,h}_{QD} = \sum_s n^{e,h}_s$. In our model, we consider only the fundamental QD transition. The level degeneracy is then $\Pi = 2$ for the two opposite spins. In addition, we neglect the transition energy difference for the exciton and biexciton states since it is usually very small compared to other broadening mechanisms that we will introduce in the following. The QD population is now $n^{e,h}_{QD} = \Pi n^{e,h}$ and the total polarization $p_{QD} = \Pi p$. In the rotating wave approximation, taking the dipole matrix element d real and introducing $p_{QD} = P_{QD}\exp(-i\omega_0 t) + c.c.$, (1,2) become

$$\frac{dP_{QD}}{dt} = -\gamma_p\left(i\Delta + 1\right) P_{QD} - \frac{idE}{\hbar}\left[n^e_{QD} + n^h_{QD} - \Pi\right] \quad (3)$$

$$\frac{dn^{e,h}_{QD}}{dt} = -\gamma_{nr} n^{e,h}_{QD} - \frac{\Gamma_{sp}}{2} n^e_{QD} n^h_{QD} + \frac{id}{\hbar}(EP^*_{QD} - E^* P_{QD}) + \left.\frac{\partial n^{e,h}_{QD}}{\partial t}\right|_{QD-WL} + \left.\frac{\partial n^{e,h}_{QD}}{\partial t}\right|_{QD-WL}^{Auger} \quad (4)$$

where we have introduced the single-dot detuning from resonance $\Delta = (\omega_a - \omega_0)/\gamma_p$.

The first QD-WL relaxation term describes the thermo-activated processes. For the sake of simplicity we ignore the possible non local interaction between the QD and the WL, drop the subscript QD in the variable names and write

$$\left.\frac{\partial n^{e,h}}{\partial t}\right|_{QD-WL} = -\gamma^{e,h}_{esc} n^{e,h} + \sigma^{e,h}_{cap} N^{e,h}_{WL}\left[\Pi - n^{e,h}\right] \quad (5)$$

where $N^{e,h}_{WL}$ is the surface density carrier population in the WL. $\gamma^{e,h}_{esc}$ and $\sigma^{e,h}_{cap}$ are respectively the escape rate from the QD and the capture rate cross-section into the QD. The second QD-WL relaxation terms describe the Auger processes [24]. For a low WL carrier density, we retain only those terms that are in first order in $N^{e,h}_{WL}$:

$$\left.\frac{\partial n^e}{\partial t}\right|_{QD-WL}^{Auger} = -B_{he} N^h_{WL} n^e\left[\Pi - n^h\right] + B_{eh} N^e_{WL} n^h\left[\Pi - n^e\right]. \quad (6)$$

The first term describes the excitation of an electron to the WL via the interaction of a hole in the WL and in the QD, and the second term is a symmetric process that describes the capture of a WL electron in the QD via the interaction of a WL and a QD hole. For the sake of conciseness, we will refer to the symmetric process in the following by ´´sym.´´ in the equations. $B_{he,eh}$ has the units of a cross-sectional rate (L^2T^{-1}). A similar term exists for the holes :

$$\left.\frac{\partial n^h}{\partial t}\right|_{QD-WL}^{Auger} = -\left.\frac{\partial n^e}{\partial t}\right|_{QD-WL}^{Auger} \quad (7)$$

Given the fast polarization decay time for the QD polarization γ_p^{-1} with respect to the other decay times, we perform an adiabatic elimination of P_{QD} in (3) and obtain :

$$P_{QD} = -\frac{id}{\hbar\gamma_p}\left(\frac{1 - i\Delta}{1 + \Delta^2}\right)\left[n^e + n^h - \Pi\right] E \quad (8)$$

Substituting in eq.(4) we obtain:

$$\frac{dn^{e,h}_{QD}}{dt} = -\gamma_{nr} n^{e,h}_{QD} - \frac{\Gamma_{sp}}{2} n^e_{QD} n^h_{QD} - \frac{2d^2}{\hbar^2\gamma_p}\left(\frac{1}{1 + \Delta^2}\right)\left[n^e + n^h - \Pi\right]|\mathbf{E}|^2 + \left.\frac{\partial n^{e,h}_{QD}}{\partial t}\right|_{QD-WL} + \left.\frac{\partial n^{e,h}_{QD}}{\partial t}\right|_{QD-WL}^{Auger} \quad (9)$$

The rate equation for the WL carrier population is given by

$$\frac{\partial N^{e,h}_{WL}}{\partial t} = \Lambda - \gamma^{WL}_{nr} N^{e,h}_{WL} + \left.\frac{\partial N^{e,h}_{WL}}{\partial t}\right|_{QD-WL} + \left.\frac{\partial N^{e,h}_{WL}}{\partial t}\right|_{QD-WL}^{Auger} + D\nabla^2_\perp N^{e,h}_{WL}. \quad (10)$$

where γ_{nr}^{WL} is the non-radiative decay term, and Λ is a pumping term. The inclusion of the latter is proposed here for sake of generality. Indeed, the electrically pumped configuration for MQW-based microresonators has proven successful to predict and observe stable CS[7,27,28]; on the other hand, ensuring a homogeneous and efficient electrical or incoherent optical pumping[29], requires a much more sophisticated architecture of the resonator, so that the first envisaged experiments will most likely be in the unpumped configuration. For such reasons, and in order to maintain this work onto a closer path to Ref.[1], the study of a pumped medium will be postponed to a future work and we shall restrict here to $\Lambda = 0$. Note the diffusion coefficient D which spreads out any initially localised excitation in the transverse plane and may contribute to diffusively couple QD at different locations. We have neglected the spontaneous emission process in the WL since we only consider first order process in N_{WL}. Considering a constant spatial density of QD N_{QD}, the Auger term and the capture term read:

$$\left.\frac{\partial N_{WL}^{e,h}}{\partial t}\right|_{QD-WL}^{Auger} = -N_{QD}\left.\frac{\partial n^{e,h}}{\partial t}\right|_{QD-WL}^{Auger}. \quad (11)$$

$$\left.\frac{\partial N_{WL}^{e,h}}{\partial t}\right|_{QD-WL} = -N_{QD}\left.\frac{\partial n^{e,h}}{\partial t}\right|_{QD-WL}. \quad (12)$$

2.2 Collection of dots

In the Stransky-Krastanov growth mode, QD have non-identical heights resulting in a broadening of the spectral linewidth of the dot ensemble. To account for this, we weigh the contribution of each class of dots by a Gaussian statistical weight:

$$G_(\Delta_i,\Delta) = \frac{1}{\Gamma/\gamma\sqrt{\pi}}\exp-\left(\Delta_i - \frac{\gamma}{\Gamma}\Delta\right)^2 \quad (13)$$

as determined by the detuning from the center ω_i of the inhomogeneously broadened line in the same manner as in [1]. We also introduce $\Delta_i = (\omega_i - \omega_0)/\Gamma$ the field detuning from the QD population line-center and Γ the inhomogeneous QD linewidth. The susceptibility of the inhomogeneously broadened QD population then stems from the summation of the responses of individual QD weighed by their Gaussian statistical contribution. The WL equation is only modified through the QD-WL interaction terms (11,12) keeping in mind that Auger or capture processes cannot involve two different dots, so that the carriers captured by all the dots (which equals the total population lost by the WL) is then just the capture rate for one spectral class of dots summed over all the distribution :

$$\left.\frac{\partial N_{WL}^{e,h}}{\partial t}\right|_{QD-WL}^{Auger} = -N_{QD}\gamma_p\times \int\left(\mp B_{eh}N_{WL}^{e,h}n^{h,e}\left[\Pi - n^{e,h}\right]\pm \text{sym.}\right)\times G_(\Delta_i,\Delta)d\Delta. \quad (14)$$

$$\left.\frac{\partial N_{WL}^{e,h}}{\partial t}\right|_{QD-WL} = -N_{QD}\gamma_p\times\int\left(-\gamma_{esc}^{e,h}n^{e,h} + \sigma_{cap}^{e,h}N_{WL}^{e,h}\left[\Pi - n^{e,h}\right]\right)\times G_(\Delta_i,\Delta)d\Delta \quad (15)$$

The field equation is obtained by following the same procedure as in [7,27]. In the mean-field limit and introducing the appropriate scalings[30], we can write the equation for the intracavity field E in an adimensional form :

$$\frac{\partial E}{\partial t} = -\left[(1+i\theta)E - E_I - i\nabla_\perp^2 E - 2C\left(\int\frac{1-i\Delta}{1+\Delta^2}(n^e + n^h - \Pi)G_(\Delta_i,\Delta)d\Delta\right)E\right]. \quad (16)$$

We have introduced $\theta = (\omega_c - \omega_0)/\kappa$, the scaled cavity-field detuning with $\kappa = cT/2n_bL$ the field decay rate, and

$$2C = \frac{d^2\omega_0 N_{QD}}{\epsilon_0\hbar\gamma_p n_b cT}. \quad (17)$$

E_I refers to the injected field while the transverse Laplacian $\nabla_\perp^2$ accounts for the diffraction inside the cavity. The time coordinate is rescaled to the field decay time κ^{-1} while the spatial transverse coordinates are rescaled to the square root of the diffraction coefficient $a = c/2n_bk_o\kappa$. L is the cavity length and k_0 is the field wavevector. The adimensional field variables are defined through the scalings $E/\sqrt{\hbar^2\gamma_p\gamma_{nr}/2d^2} \rightarrow E$ and $-i\sqrt{RT\hbar^2\gamma_p\gamma_{nr}/2d^2}$ with $T = 1 - R$ the mirror mean transmittivity. Recalling that the intensity absorption coefficient is related to the susceptibility χ by $\alpha = -\omega_0\Im m[\chi]/cn_b$, with n_b the background refractive index, it is easy to see that C has the dimension of $\alpha L/T$ and is therefore related, as expected, to the ratio of absorptive loss to cavity losses. The carrier equations can also straightforwardly be recast in an adimensional form using the following scalings : $\gamma_{nr}/\kappa \rightarrow \gamma$, $\Gamma_{sp}/\gamma_{nr} \rightarrow \Gamma, \gamma_pG \rightarrow G, \gamma_{esc}^{e,h}/\gamma_{nr} \rightarrow \gamma_{esc}^{e,h}, \sigma_{cap}^{e,h}N_{QD}/\gamma_{nr} \rightarrow \sigma_{cap}^{e,h}, \gamma_{nr}^{WL}/\kappa \rightarrow \gamma_{nr}^{WL}, \Lambda/N_{QD}\gamma_{nr}^{WL} \rightarrow \Lambda, \Gamma_{sp}^{WL}N_{QD}/\gamma_{nr}^{WL} \rightarrow \Gamma_{sp}^{WL}$, $D/a\gamma_{nr}^{WL} \rightarrow D$ and $B_{eh,he}N_{QD}/\gamma_{nr} \rightarrow B_{eh,he}$. The WL carrier population $N_{WL}^{e,h}$ has been rescaled to the total QD density N_{QD}.

With these rescalings eq.s (9) for electrons and holes, and eq.s (10) for the WL become:

$$\frac{dn_{QD}^{e,h}}{dt} = -\gamma \left[n^{e,h} + \frac{\Gamma_{sp}}{2} n^e n^h + \frac{|\mathbf{E}|^2}{1+\Delta^2} \left[n^e + n^h - \Pi \right] \right.$$
$$\pm B_{he} N_{WL}^h n^e \left[\Pi - n^h \right] \mp B_{eh} N_{WL}^e n^h \left[\Pi - n^e \right]$$
$$\left. + \gamma_{esc}^{e,h} n^{e,h} - \sigma_{cap}^{e,h} N_{WL}^{e,h} \left[\Pi - n^{e,h} \right] \right] \quad (18)$$

$$\frac{\partial N_{WL}^{e,h}}{\partial t} = -\gamma^{WL} \left[-\Lambda + N_{WL}^{e,h} - D\nabla_\perp^2 N_{WL}^{e,h} \right.$$
$$\mp B_{he} N_{WL}^h \int n^e \left[\Pi - n^h \right] G_(\Delta_i, \Delta) d\Delta$$
$$\pm B_{eh} N_{WL}^e \int n^h \left[\Pi - n^e \right] G_(\Delta_i, \Delta) d\Delta$$
$$- \gamma_{esc}^{e,h} \int n^{e,h} G_(\Delta_i, \Delta) d\Delta$$
$$\left. - \sigma_{cap}^{e,h} N_{WL}^{e,h} \int \left[\Pi - n^{e,h} \right] G_(\Delta_i, \Delta) d\Delta \right] \quad (19)$$

Equations (18) for the electrons and holes and (19) for the WL with eq. (16) for the field are the final equations to study.

3 Numerical results

3.1 Steady-state and stability analysis

In the limit of a pure optical generation of carriers (passive configuration of the system) provided by the injected beam, and neglecting the QD-WL interactions (r.h.s of (5,6) set to zero), we remark that it is possible to consistently reduce the present model to our previous two-level model (TLM) discussed in [1] by setting $n^e(\omega) + n^h(\omega) = 2n$ (i.e. a two-level system in the excited state contributes to both an electron and a hole so that the TLM bistability parameter C_{TLM} is twice our present C parameter). Rewriting our model with the above-mentioned simplifying assumptions, it is possible to recast it to the two-level, inhomogeneously broadened model, thus assessing the consistency of our approach. Reintroducing the QD-WL interaction terms in the absence of the pump ($\Lambda = 0$), we have evaluated the role of the Auger effect and radiative recombination. The steady-state values of the field and the electron and holes densities are basically independent of these terms. It can be understood, as discussed in the previous section, in terms of the moderate carrier density in the WL and the QD. On the contrary, the stationary curves and the domains of modulational instability are more significantly influenced by the QD-WL relaxation mechanisms ($\gamma_{esc}^{e,h}$ and $\sigma_{cap}^{e,h}$ terms). We will study both the focusing and defocusing regimes. We note here that a negative or a positive value of Δ_i is loosely referred to as "focusing" or "defocusing" respectively in the sense that most of the classes of QD lie on the focusing or defocusing side of the injected frequency.

We tried to keep as close as possible to the regimes studied in [1], while compromising for the most promising indications for stable solitonic branches. We thus considered

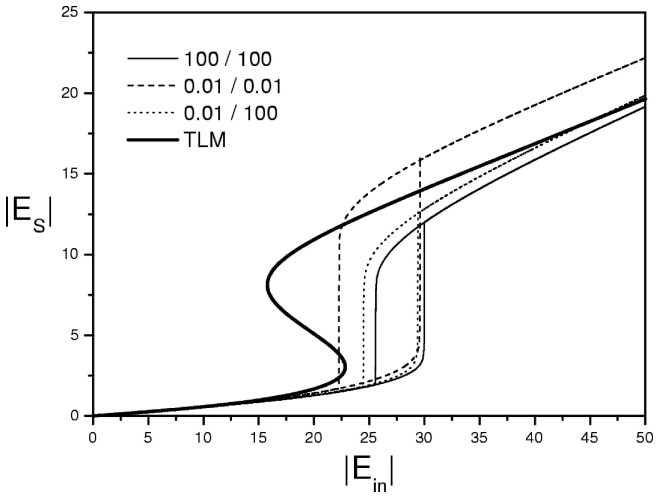

Figure 1 Homogeneous steady state curves obtained via a sweep process for the focusing parameter set (see text) and various combinations of the escape rates $\gamma_{esc}^e/\gamma_{esc}^h$ corresponding to the good, intermediate and poor confi nement cases. The black S-curve refers to the TLM for $\theta = -3$, $\Delta_i = -1$, $\gamma = 15$, $\Gamma = 60$, $C_{TLM} = 20$.

the following set of parameters: for the focusing one $\sigma_{cap} = 500$,$\theta = -3$, $\Delta_i = -1$, $\gamma = 15$, $\Gamma = 60$, $C = 20$, $B_{he,eh} = 500$, $\Gamma_{sp} = 2.5$, $D = 0.41$, $\Lambda_{pump} = 0$. For the defocusing regime parameters are as for the previous case except for $\Delta_i = 0.5$, $\theta = -2$ and $C = 35$. The choice of the values of C will be clarified later. We studied three physical situations corresponding to a good carrier confinement inside the QD ($\gamma_{esc}^e = \gamma_{esc}^h = 0.01$), a poor one ($\gamma_{esc}^e = \gamma_{esc}^h = 100$), and finally an intermediate situation where the hole confinement is weaker than that of the electrons because of an unbalanced band-offset ratio ($\gamma_{esc}^h = 100$, $\gamma_{esc}^e = 0.01$). By inspecting the steady state curves reported in fig.(1) we interpret the effect of the different escape/capture rates on the nonlinear medium response as follows: an increased escape rate, corresponding to a reduced contribution to the QD optical susceptibility, shifts the hysteresis cycle towards higher values for the input intensity, and yields lower intracavity intensities. On the contrary, lower escape rates bring the stationary response of the system closer to the case of Ref. [1] where the WL was not accounted for. Although not discussed here, in the details of the simulations, similar considerations hold for the variation of the capture rates. We also performed some numerical simulations in the intermediate confinement regime with different values of the $B_{eh,he}$ coefficients. The characteristic curves of the system steady-state response are indistinguishable with $B_{he} = 500$ and $B_{eh} = 1000, 500, 50, 0$. The sets of parameters $B_{he} = 0$ and $B_{eh} = 0, 1000$ leads also to near identical results too. Both results are however close because Auger processes are perturbative in this model, since the WL populations are low. We have nevertheless chosen the parameters $B_{he,eh} = 500$ since it leads to a somewhat higher bistability range while applying to a wide range of B_{eh} values too.

The steady-state curves of fig.1 were obtained by two different numerical approaches : by integrating our rate equa-

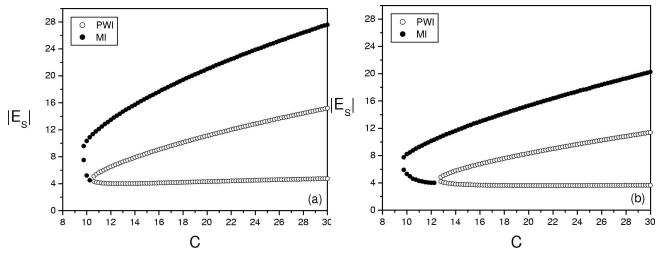

Figure 2 Focusing regime. PWI and MI boundaries vs C in the good (a) and poor (b) confi nements cases.

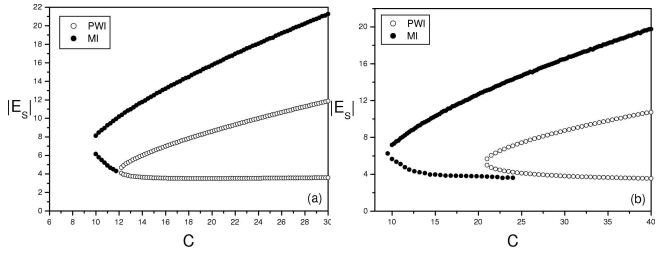

Figure 3 PWI and MI boundaries vs. C in the intermediate confi nement case for the focusing (a) and defocusing (b) set of parameters letting C vary. The vertical line corresponds to the specifi c values of C that are chosen for the pattern formation analysis. The intersection of this line with the MI and PWI boundaries make it possible to infer the unstable portion of the homogeneous curve.

tions, cancelling Laplacian terms, or by using the intracavity intensity as a dummy parameter. The two methods are in perfect agreement and also provided indications on the input field variation timescale to produce an acceptable adiabatic sweep of the field dynamics. In all the subsequent figures we rely on this second method to reproduce, when necessary, the steady state homogeneous curves. The linear stability analysis cannot be obtained algebraically and thus a simple expression for the Turing instability boundaries cannot be derived. Nonetheless an analysis of the instabilities can be performed in a numerical way. The search for plane wave instabilities (PWI), i.e. instabilities against a plane homogeneous perturbation, is quite straightforward since it consists in finding the region of negative slope in the homogeneous steady state curve. In order to study the modulational instabilities (MI) caused by transversely modulated perturbations we rely on the direct numerical simulations of the full equations (i.e. with the diffraction and diffusion operators). The simulations were performed adopting only one transverse dimension instead of two, since it is known (and we anyway cross-checked our evidences) that, while the patterns emerging at steady-state from a MI as well as their stability scheme are obviously influenced by the spatial dimensionality, the instability boundaries are independent of the Laplacian dimensions and only depend on the modulus of the transverse wavevector.

In fig.2 and 3, we plot the values of $|E_S|$ corresponding to MI and PWI boundaries for different values of C in the focusing and defocusing regimes.

The role played by the escape rates of electrons and holes is illustrated in fig.2 by the dependence of the critical C parameter for MI and PWI. Low escape rates tend to strengthen the non-linear interaction and this determines a bistable behavior for values of C down to 10. This case is also very close, as expected, to the TLM (fig.4(a) of[1]) because both electrons and holes last long in their excited states and the whole system is indeed similar to a TLM. The quantitative comparison is satisfactory provided that we recall that $C_{TLM} = 2C$. On the contrary for the poor confinement case, bistability starts at $C = 13$. In both cases the lower branch of the bistable curve is stable and a consistent portion of the upper branch is unstable versus modulated perturbations. In the slightly defocusing regime with $\Delta_i = 0.5$ and $\theta = -2$, we have observed an opposite behavior with respect to the focusing regime. The good confinement case is very similar to the TLM results in fig.4(b) of [1] and the onset of bistability is for $C > 45$. By contrast, for the intermediate and poor confinement cases the onset of bistability is for $C > 20$. By inspecting fig.3(b) we see that, when the system is bistable, a fairly large portion of the upper homogeneous branch is modulationally unstable, and for $C > 30$ the whole lower branch is basically stable. This behavior is quite different from the defocusing regime of the TLM (see fig. 4(b) in [1]) where it appeared that even for $C_{TLM} \leq 100$, a considerable portion of the lower branch was affected by the MI. The inclusion of QD-WL interactions seems to stabilize the lower homogeneous branch, possibly via the phenomenon of carrier diffusion in the WL.

In order to appreciate the new features that emerge when considering QD-WL interactions, we consider for both the focusing and defocusing regimes the intermediate confinement case ($\gamma^e_{esc} = 0.01$,$\gamma^h_{esc} = 100$). On the basis of previous studies on cavity solitons, we are aware of some necessary or favorable conditions for the existence of cavity solitons. In particular, a bistable homogeneous curve and an MI affecting a large portion of the upper branch are highly desirable to obtain stable cavity solitons. In addition, when the stationary curve is bistable, stability of the lower branch is a necessary condition. In the following we will meet these conditions by a proper choice of the bistability parameter C both for the focusing and defocusing regime.

4 Patterns and Cavity solitons: simulations

The dynamical equations have been numerically integrated by means of a split-step method with periodic boundary conditions. All the integrals have been calculated by discretizing the spectral distribution of n_e and n_h in a suitable partition.

The pattern zoology depends on the regime, focusing or defocusing, considered. We studied the branches of patterns emerging from the MI and followed the changes thereof. We identified the branches of stable cavity solitons (CS) checking not only their long-term stability, but also their independence/addressability in the sense that they were written and erased by the pulse addressing technique [27].

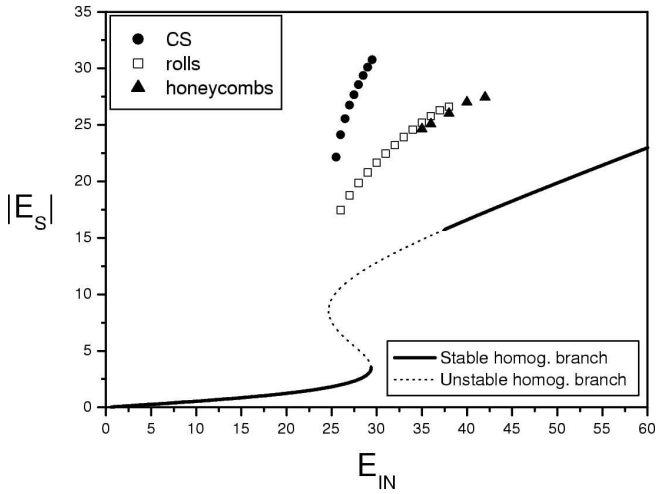

Figure 4 Focusing Regime. Steady state curve of the homogeneous solutions and results of numerical simulations of the full equations in the intermediate confi nement regime. Patterns are indicated by different symbols whose ordinate corresponds to the maximum intracavity fi eld amplitude in the pattern.

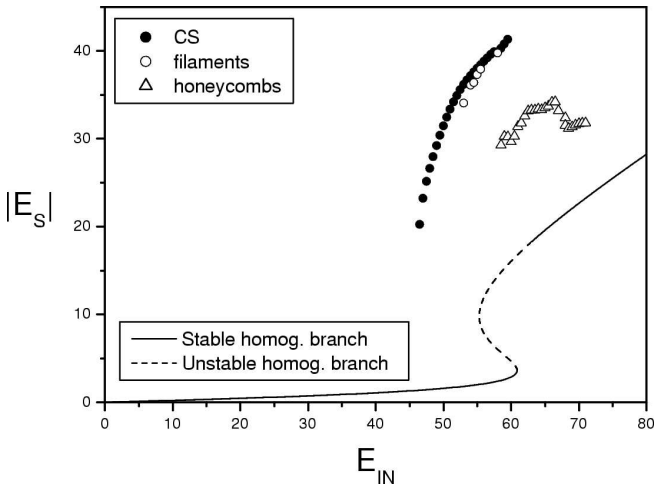

Figure 5 Defocusing Regime. Steady state curve of the homogeneous solutions and results of numerical simulations of the full equations in the intermediate confi nement regime. Patterns are indicated by different symbols whose ordinate corresponds to the maximum intracavity fi eld amplitude in the pattern.

4.1 Focusing regime

In fig.3(a) the PWI and MI boundaries as function of C are shown, and in fig.4 we report the bistability curve with a complete characterization of patterns arising as self-organized structures and of CS. Honeycomb patterns are met subcritically beyond the onset of the MI on the upper branch of the homogeneous curve; they exist for values of the input field amplitude in the range 35 - 42. Decreasing the input field, honeycomb destabilize in favour of roll patterns. They exist for a sizable range of the input field amplitude and evolve to ensembles of localized structures when the input field amplitude is decreased below 31. Stable CS are found from 25.5 up to the value of the input field corresponding to the lower homogeneous branch turning point (see vertical line in fig.4: this is a general feature of CS since they need a stable lower branch on which sit. The patterns observed are qualitatively comparable with those predicted in other nonlinear resonators and their general scheme of evolution and competition is similar to previous studies [27, 31].

4.2 Defocusing regime

In contrast to what is usually observed, the defocusing regime (see fig.5) does not seem to be less favourable than the focusing one to the occurrence of CS, at least for our parameter choice. With respect to the focusing case on fig.4 there is a shift of the viable/interesting regimes towards higher field values but on the overall the pattern branches are quite similar. This is an indication that for the defocusing regime one can still expect stable structures and CS. Indeed with the choice $\Delta_i = 0.5$, which corresponds to a slight defocusing effect, the absorptive behavior dominates over the dispersive one and this, as it will become evident in the pattern morphology, counterbalance the overall defocusing effect. The vertical line reported in fig.3(b) allows us to identify the values of the intracavity field that correspond to the unstable portion of the homogeneous steady state curve reported in fig.5. We report also a characterization of patterns and CS. Here we find again honeycombs that subcritically emerge beyond the onset of MI on the upper homogeneous branch. However, at difference from the focusing regime, their stabilization is not complete over the entire transverse plane, but is characterised by the presence of persistent defects. By lowering the input field these defects tend to alter the whole correlation among the elementary cells of the patterns, and for input field amplitude lower than 58.5 the self organized honeycomb pattern loose stability in favour of irregular, transverse filaments. Filaments are not stable patterns but they endlessly move in the transverse plane: eventually for input amplitude lower than 53 they fragment in multiple ensembles of CS.

We have observed that everywhere such spontaneously organised CS are stable, we could also independently address and switch on/off CS by means of narrow Gaussian pulses, superimposed to the homogeneous background, centered at the point at which we want to create or annihilate the CS. The CS stable branch extends in the range 46.5 - 60 of the input field amplitude. We note that this range of existence is broader than that found for the focusing regime. So, both regimes might in principle be adopted for an experimental search for CS in such systems.

5 Conclusion

In this paper, we have developed an extended model for the description of the optical response of a semiconductor QD medium in a cavity. This model complements the previously

studied effects of inhomogeneous broadening (a specific feature reflecting the fluctuations of the QD size) with the microscopic mechanisms coupling the QD itself with the thin quantum well on which it sits such as thermal capture and emission, and Auger scattering. We considered regimes of moderate coherent optical excitation, where we have been able to properly calculate the optical response and confirm the ability of such a material system to exhibit focusing as well as defocusing nonlinearities, depending on the spectral detuning of light with respect to the inhomogeneous line center. We have applied this model to the analysis of self-organizing optical properties such as periodic pattern and cavity soliton formation. The conditions for the onset of MI and new bifurcated branches clearly express the favourable character of focusing nonlinearities on assisting the absorption saturation mechanisms in this process, while denoting that still acceptable conditions can be found in the moderately defocusing case. We showed that escape processes between the WL and the QD affect only moderately the thresholds and the intensities needed for CS formation. This result is encouraging in view of practical implementations of QD in high finesse cavities for pattern and CS formation in the focusing regime. More unexpectedly, the defocusing regime shows somewhat more favourable than in [1] to the stable appearance of CS through the stabilization of the lower branch. This effect can be attributed to the presence of a small carrier diffusion mediated by the WL between the QD, which is known to improve the stability range of CS[27]. Our model can also describe a pumped QD medium with, if needed, additional Auger mechanisms corresponding to higher excitation densities, although this study is left to future work.

Acknowledgements

Authors acknowledge the partial support from the European Commission through the STREP project N.004868 (FunFACS). In addition, S.B. and R.K. wish to acknowledge partial support from the Région Ile de France.

References

1. S. Barbay et al., IEEE J. Quantum Electronics **39**, 245 (2003).
2. R. Kuszelewicz, I. Ganne, I. Sagnes, G. Slekys, and M. Brambilla, Phys. Rev. Lett. **84**, 6006 (2000).
3. I. Ganne and G. Slekys and I. Sagnes and R. Kuszelewicz, Phys. Rev. E **66**, 066613 (2002).
4. V. Taranenko, I. Ganne, R. Kuszelewicz, and C. Weiss, Phys. Rev. A **61**, 063818 (2000).
5. M. Segev, B. Crosignani, A. Yariv, and B. Fischer, Phys. Rev. Lett. **68**, 923 (1992).
6. N. Fressengeas, J. Maufoy, and G. Kugel, Phys. Rev. E **54**, 6866 (1996).
7. M. Brambilla, L.A. Lugiato, F. Prati, L. Spinelli, and W. Firth, Phys. Rev. Lett. **79**, 2042 (1997).
8. P.L. Ramazza, S. Ducci, S. Boccaletti, and F.T. Arecchi, J. Opt. B: Quantum Semiclass. Opt. **2**, 399 (2000).
9. S. Residori, A. Petrossian, T. Nagaya, and M. Clerc, J. Opt. B: Quantum Semiclass. Opt. **6**, S169 (2004).
10. B. Schaepers, T. Ackemann, and W. Lange, IEEE J. Quantum Electronics **39**, 227 (2003).
11. F. Adler et al., J. Appl. Phys. **80**, 4019 (1996).
12. K. Mukai, N. Ohtsuka, H. Shoji, and M. Sugawara, Appl. Phys. Lett. **68**, 3013 (1996).
13. M. Grundmann and D. Bimberg, Phys. Rev. B **55**, 9740 (1997).
14. W. W. Chow, H. C. Schneider, and M. C. Phillips, Phys. Rev. A **68**, 053802 (2003).
15. H.C. Schneider, W.W. Chow, and S.W. Koch, Phys. Rev. B **64**, 115315 (2001).
16. H. C. Schneider, W. W. Chow, and S. W. Koch, Phys. Rev. B **66**, 041310 (2002).
17. W.W. Chow and H.C. Schneider, Appl. Phys. Lett. **81**, 2566 (2002).
18. H. C. Schneider, W. W. Chow, and S. W. Koch, Phys. Stat. Sol. (b) **238**, 589 (2003).
19. E. Gehrig and O. Hess, Phys. Rev. A **65**, 033804 (2002).
20. A.V. Uskov et al., Appl. Phys. Lett. **84**, 272 (2004).
21. S.P. Hegarty, B. Corbett, J.G. McInerney, and G. Huyet, Electron. Lett. **41**, 416 (2005).
22. M. Paillard et al., Phys. Rev. Lett. **86**, 1634 (2001).
23. E. Tsitsishvili, R. v. Baltz, and H. Kalt, Phys. Rev. B **66**, 161405 (2002).
24. A. V. Uskov, J. McInerney, F. Adler, H. Schweizer, and M. H. Pilkuhn, Appl. Phys. Lett. **72**, 58 (1998).
25. A. V. Uskov and K. Nishi and R. Lang, Appl. Phys. Lett. **74**, 3081 (1999).
26. W. W. Chow, S. W. Koch, and M. Sargent III, *Semiconductor-Laser Physics*, Springer-Verlag, 1994.
27. L. Spinelli, G. Tissoni, M. Brambilla, F. Prati, and L. Lugiato, Phys. Rev. A **58**, 2542 (1998).
28. S. Barland et al., Nature **419**, 699 (2002).
29. S. Barbay, Y. Ménesguen, I. Sagnes, and R. Kuszelewicz, Appl. Phys. Lett. **86**, 151119 (2005).
30. L. Spinelli, *Cavity solitons in semiconductor microresonators: applications to all-optical information technology*, PhD thesis, 1998.
31. G. Tissoni et al., J. Opt. Soc. Am. **16**, 2095 (1999).